



HAL
open science

Study on the self-shielding and temperature influences on the neutron irradiation damage calculations in reactors

Shengli Chen, David Bernard, Laurent Buiron

► **To cite this version:**

Shengli Chen, David Bernard, Laurent Buiron. Study on the self-shielding and temperature influences on the neutron irradiation damage calculations in reactors. Nuclear Engineering and Design, 2019, 346, pp.85-96. 10.1016/j.nucengdes.2019.03.006 . cea-02535265

HAL Id: cea-02535265

<https://cea.hal.science/cea-02535265>

Submitted on 22 Oct 2021

HAL is a multi-disciplinary open access archive for the deposit and dissemination of scientific research documents, whether they are published or not. The documents may come from teaching and research institutions in France or abroad, or from public or private research centers.

L'archive ouverte pluridisciplinaire **HAL**, est destinée au dépôt et à la diffusion de documents scientifiques de niveau recherche, publiés ou non, émanant des établissements d'enseignement et de recherche français ou étrangers, des laboratoires publics ou privés.



Distributed under a Creative Commons Attribution - NonCommercial 4.0 International License

Study on the self-shielding and temperature influences on the neutron irradiation damage calculations in reactors

Shengli Chen^{1,2,*}, David Bernard¹, Laurent Buiron¹

¹ CEA, Cadarache, DEN/DER/SPRC/LEPh, 13108 Saint Paul Les Durance, France

² Université Grenoble Alpes, I-MEP2, 38402 Saint Martin d'Hères, France

* Corresponding author: shengli.chen@cea.fr

Abstract

Displacement per Atom (DPA) is conventionally computed using the DPA cross sections in reactor applications. The DPA cross sections can be influenced by temperature through the Primary Knocked-on Atom (PKA) energy and the Doppler broadening of reaction cross sections. The former is shown not important due to the threshold energy of atomic displacement and the small value of thermal kinetic energy. For ⁵⁶Fe, the Doppler broadening has limited influence on DPA cross sections due to high resonance energies. On the other hand, the self-shielding should be considered in the computation of DPA, which depends not only on the cross sections but also the corresponding recoil energies of the PKA. ECCO 1968-group calculations show that the self-shielding corrections on DPA cross sections are necessary for the computation of atomic displacement. In addition, the total DPA rate calculated by self-shielding corrected total cross sections is smaller than the sum of the above three components. The recommended method to compute DPA is the calculation of each reaction, especially for coarse energy structures. The total DPA rate in ASTRID reactor inner core is 25 DPA/year, for which the contributions of the elastic scattering, total inelastic scattering, and disappearance reactions are 81.9%, 18.0%, and 0.1%, respectively. The corresponding relative reductions due to the corrections of multi-group cross sections are 11.3%, 5.9%, and 20.5%, respectively.

Keywords: Self-shielding, DPA, Recoil energy, Doppler effect, ASTRID

1. Introduction

The neutron irradiation induced embrittlement is one of the major materials challenges of the Reactor Pressure Vessels (RPV) [1] due to the change of mechanical behaviors by irradiation. The Displacement per Atom (DPA) defines the average number displacements of each atom under irradiation. It is one of the key parameters to measure the irradiated damage. The lifetime of the current water reactors is mainly

determined by the accumulated DPA number of the RPV. For fast neutron reactors, the cycle length depends on the DPA. In sodium-cooled fast reactors, the DPA in the fuel cladding is more important than that of the reactor vessel because of the shielding by fertile layer, reflector, and large volume of sodium (and in-vessel neutron shielding in ASTRID [2]) between the inner core and the reactor vessel.

When kinematic particles knock-on an atom in materials, a Frenkel pair (an atomic vacancy combined with an interstitial) is formed. The knocked-on atom is able to induce more crystallographic defects through atomic displacement cascades. Various models have been developed to compute the average DPA number using the Primary Knock-on Atom (PKA) energy as a major parameter, including Molecular Dynamics (MD) simulations and the classical DPA formulae. Many works performed with MD simulations show that the DPA depends on temperature (decreases with temperature due to the increase of recombination of displaced atoms with irradiation temperature) [3]–[6]. Gao's work shows about 20%-30% decrement of DPA as the irradiation temperature increases from 100 K to 900 K for α -iron [3]. However, Phythian concluded the weak dependence of residual defects on temperature for the copper and iron [4]. Phythian's conclusion on iron is later verified by Stoller [5]. The present work investigates the temperature effects on DPA by considering the influence of irradiation temperature on recoil energy and Doppler broadening.

For computation of DPA rates in reactors, the typical method is using DPA cross sections and the corresponding spectra of incident particles. Neutron-induced DPA cross sections are calculated with nuclear data by processing codes as NJOY [7]. The corresponding spectra of incident particles are determined by the transport codes. The two above-mentioned effects of the temperature: (i) the influence on PKA energy due to the thermal vibration of atoms (i.e. exit channel Doppler broadening), and (ii) Doppler broadening of reaction cross sections (i.e. entrance channel Doppler broadening) are considered in the calculation of DPA cross sections. The dependence of spectra on temperature is automatically taken into account in transport codes.

In the compound nucleus theory, the reaction cross section has a peak value when the energy of the compound system is close to one of the excited levels of the compound nucleus. This phenomenon is referred to resonance. Due to the huge cross section in the vicinity of resonance energy, the corresponding neutron spectrum has a local valley at the same energy band. This is the resonance self-shielding, referred simply hereinafter to self-shielding. In deterministic neutron transport codes, due to the finite background cross section at resonance energies, one has to decrease resonant cross sections within the multi-group formalism. This leads to an increase of the multi-group neutron flux at resonant energies to conserve the reaction rate. Many methods have been proposed to treat the self-shielding in the deterministic codes. However, the self-shielding effect is rarely treated in DPA calculations, while DPA is one of the most important characters to measure the properties of materials under irradiation. The present work studies the influence of self-shielding on DPA calculations.

The Stainless Steel (SS) is widely used in the nuclear industry, such as the reflector and the RPV in Light Water Reactors (LWRs), fuel cladding of fast reactors. Recent studies also show that the SS can be a potential fuel cladding material for Accident

Tolerant Fuel (ATF) in LWRs [8], [9]. The abundance of ^{56}Fe in natural iron is 91.75%, while iron is the main element in SS. Therefore, the numerical results shown in the present work are based on ^{56}Fe . The neutronic calculations are performed with the deterministic code ERANOS-2.3 [10]. The calculations of DPA rates are based on the fuel cladding of the inner core in the Advanced Sodium Technological Reactor for Industrial Demonstration (ASTRID) [2]. All simulations are based on the JEFF-3.1.1 nuclear data library [11]. The DPA cross sections are computed with the modified HEATR module in NJOY-2016.20 [12]. The modification in HEATR module for DPA calculations is described in Ref. [13]: the second ‘‘stair’’ in DPA metrics (c.f. Section 2.1: 1 DPA for damage energy between E_d and $2.5E_d$) is added, while the formula above $2.5E_d$ is used by NJOY in this interval.

2. Methods

2.1 DPA metrics

In nuclear reactor applications, the DPA metrics are used to compute the DPA cross sections. Based on elastic scattering among hard spheres, Kinchin and Pease proposed the KP-DPA in 1955 [14]. The current international standard is the Norgett-Robinson-Torrens (NRT)-DPA model [16]:

$$N(E_a) = \begin{cases} 0, & 0 < E_a < E_d \\ 1, & E_d < E_a < 2E_d/0.8 \\ \frac{0.8E_a}{2E_d}, & 2E_d/0.8 < E_a < \infty \end{cases}, \quad (1)$$

where E_a is the Lindhard’s damage energy [15], E_d is the angle-averaged threshold energy of atomic displacement, and the constant coefficient 0.8 is deduced from the Binary Collision Approximation (BCA) calculations [17]. The damage energy is computed with the PKA kinetic energy E_{PKA} by $E_a = E_{PKA} \times P(E_{PKA}/E_L)$, where P is the partition function that measures the fraction of E_{PKA} left in atomic motion ($1 - P$ represents the fraction of energy lost to electronic excitation) [18]:

$$P(\varepsilon) = 1/[1 + k(3.4008\varepsilon^{1/6} + 0.40244\varepsilon^{3/4} + \varepsilon)], \quad (2)$$

where $k = 0.133745Z^{2/3}A^{-1/2}$, $\varepsilon = E_{PKA}/E_L$ with $E_L = 86.931Z^{7/3}$ (in eV), Z and A are respectively the atomic number and the atomic mass number. The average threshold energy for the iron isotopes is 40 eV [19].

However, the NRT model overestimates the atomic displacement [20]. Taking the athermal recombination of displaced atoms into account, the Athermal Recombination-Corrected (ARC)-DPA is proposed [21]:

$$N(E_a) = \begin{cases} 0, & 0 < E_a < E_d \\ 1, & E_d < E_a < 2E_d/0.8 \\ \frac{0.8E_a}{2E_d} \xi(E_a), & 2E_d/0.8 < E_a < \infty \end{cases}, \quad (3)$$

where

$$\xi(E_d) = (1 - c) \times \left(\frac{0.8E_d}{2E_d}\right)^b + c, \quad (4)$$

where b and c are fitting coefficients. Assuming $E_d = 40$ eV, Ref. [21] recommends $c = 0.286$ and $b = -0.568$ for iron isotopes according to molecular dynamics simulations.

2.2 Recoil energy of PKA

The recoil energy of PKA is fundamental for DPA calculations. Figure 1 shows the scheme of the collision in the Laboratory (Lab) frame. The incident and emitted kinetic energies are referred to E and E' , respectively. E_R stands for the recoil energy of the target nucleus. m and v (m' and v') are respectively the mass and velocity of the incident (outgoing) particle. The kinetic energy of the target is set to $1.5kT$, which is the average kinetic energy for particles with temperature T . $k = 8.617 \times 10^{-5}$ eV/K is the Boltzmann constant. θ denotes the angle of the target due to thermal vibration. The angle between the velocity of Center-of-Mass (CM) and the incident direction is denoted by φ . The emission angle is referred to α . The emission angle in the CM frame is noted as α_c .

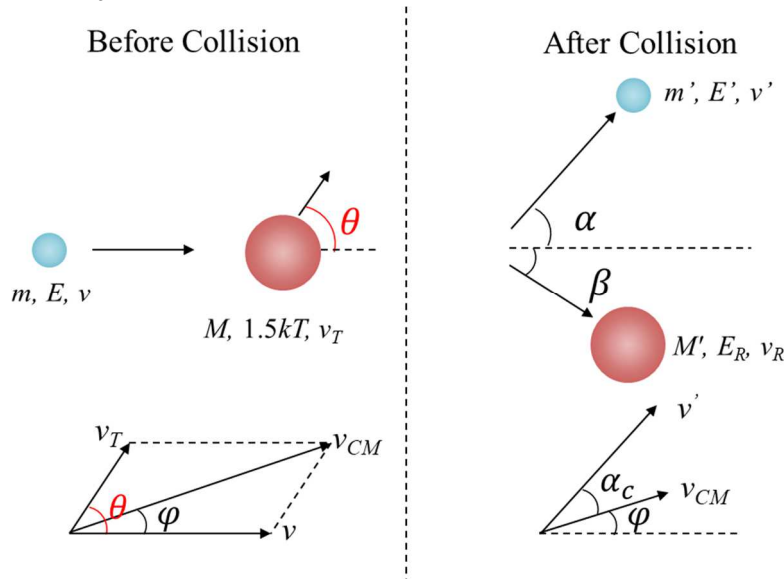


Figure 1. Scheme of the collision in the Laboratory frame

The conservation of energy conducts to:

$$E + 1.5kT = E' + E_R + Q, \quad (5)$$

where Q is the reaction energy. The conservation of momentum before and after collision shows:

$$mv + Mv_T \cos \theta = m'v' \cos \alpha + M'v_R \cos \beta, \quad (6)$$

$$Mv_T \sin \theta = m'v' \sin \alpha + M'v_R \sin \beta. \quad (7)$$

At low incident energies, the emission in the CM α_c is supposed to be isotropic. At high energies, the angular distribution can be found in Evaluated Nuclear Data Files (ENDF), which often gives the distribution of α_c . The angular distribution of α can be determined by that of α_c and φ because $\alpha = \alpha_c + \varphi$. The conservation of momentum before collision leads to:

$$mv + Mv_T \cos \theta = (m + M)v_{CM} \cos \varphi, \quad (8)$$

$$Mv_T \sin \theta = (m + M)v_{CM} \sin \varphi. \quad (9)$$

φ satisfies thus:

$$\tan \varphi = \frac{Mv_T \sin \theta}{mv + Mv_T \cos \theta}. \quad (10)$$

Due to the symmetry, one can further suppose that $\theta \in [0, \pi]$. Consequently, for $mv > Mv_T$, i.e. $mE > 1.5MkT$,

$$\varphi = \tan^{-1} \left(\frac{Mv_T \sin \theta}{mv + Mv_T \cos \theta} \right). \quad (11)$$

The recoil energy depends on the angle of thermal vibration θ . However, it is not so important to study the dependence of recoil energy on θ because the latter has to be random. The random value of θ leads to the isotropic angular distribution. Therefore, the recoil energy averaged over θ is investigated. The isotropic angular distribution of θ conducts to:

$$E_R(E, T, \alpha_c) = \frac{1}{2} \int_{-1}^1 E_R(E, T, \alpha_c, \theta) d(\cos \theta). \quad (12)$$

2.3 DPA calculations in reactors

The DPA rate induced by a particle other than atoms in the material is calculated by:

$$DPA = \int_0^\infty \sum_i \frac{0.80}{2E_d} \times [\bar{E}_{a,i}(E) \sigma_i(E)] \phi(E) dE, \quad (13)$$

where the index i reveals the reaction types, such as elastic scattering and inelastic scatterings. $\sigma_i(E)$ is the cross section of the reaction i at energy E , $\phi(E)$ refers to the flux of incident particle, and $\bar{E}_{a,i}(E)$ is the corresponding damage energy computed by:

$$\bar{E}_{a,i}(E) = \int_0^\pi E_a(E, \alpha_c) \xi(E_a(E, \alpha_c)) f(E, \alpha_c) d\alpha_c, \quad (14)$$

where the displacement efficiency $\xi = 1$ for NRT-DPA and Eq. (4) for ARC-DPA, $f(E, \alpha_c)$ is the angular distribution for the emission particle. More details can be found in Ref. [13] and [22] for discrete reaction channels and continuum reactions, respectively.

In a reactor core, the upper limit of the integral in Eq. (13) is 20 MeV. $\sigma_{DPA,i}(E) = \bar{E}_{a,i}(E) \sigma_i(E)$ is the DPA cross section (in barn.eV) induced by the reaction type i at incident energy E as shown in Figure 6, which illustrates the total, elastic scattering, total inelastic scattering, and disappearance DPA cross sections (MT444, MT445, MT446, and MT447, respectively) for ^{56}Fe at 293.15 K. The disappearance DPA cross section is the sum of DPA caused by reactions without neutron emission, i.e. reactions from MT102 to MT120. For ^{56}Fe in JEFF-3.1.1, only the cross sections from MT102 to MT107 are evaluated. The processing and the reliability of the elastic and discrete inelastic scatterings (continuum inelastic scattering, respectively) with nuclear data are investigated in Ref. [13] (Ref. [22], respectively). The disappearance signifies no neutron emission after reaction, such as (n, γ), (n,p), and (n, α) reactions. It is noticeable

that the DPA rates induced by reactions excluded in MT445-447, e.g. (n,2n) and (n,np), are quite neglectable (values shown in the caption of corresponding figures of DPA rates).

Figure 2 illustrates the different routines of DPA calculations. Eq. (13) is the method of DPA calculation without considering the self-shielding correction (green scheme in Figure 2). As mentioned in Section 1, both cross sections and neutron flux are modified in deterministic codes due to the self-shielding treatment. The DPA rate after the correction of self-shielding is calculated by:

$$DPA = \int_0^{20MeV} \sum_i \frac{0.80}{2E_d} \times [\bar{E}_{a,i}(E) \tilde{\sigma}_i(E)] \tilde{\phi}(E) dE, \quad (15)$$

where $\tilde{\sigma}$ and $\tilde{\phi}$ represent cross sections and neutron flux with the correction of self-shielding. The neutron flux mentioned in the following description is the neutron flux after the correction of self-shielding, ϕ will be thus used rather than $\tilde{\phi}$ to simplify the notation. Hence, the DPA rate can be calculated by:

$$DPA = \frac{0.80}{2E_d} \times \int_0^{20MeV} \sum_i \sigma_{DPA,i}(E) \frac{\tilde{\sigma}_i(E)}{\sigma_i(E)} \phi(E) dE. \quad (16)$$

Discretizing the integral to the sum of multi-group structure:

$$DPA = \frac{0.80}{2E_d} \times \sum_{j=1}^G \sum_i \sigma_{DPA,i,j} \frac{\tilde{\sigma}_{i,j}}{\sigma_{i,j}} \phi_j. \quad (17)$$

where G is the number of groups, $\tilde{\sigma}_{i,j}$ denotes the self-shielding corrected multi-group reaction cross section. This method corresponds to the red routine illustrated in Figure 2.

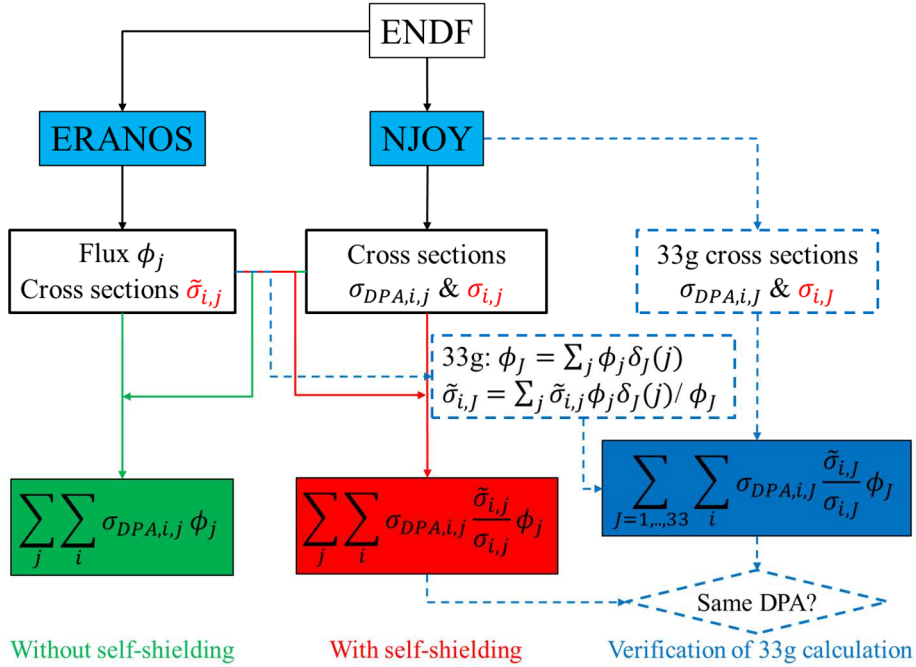


Figure 2. Flowchart of DPA calculations without (green) and with (red) self-shielding corrections. The dashed scheme is only for the verification of ECCO 33-group calculations by using multi-group cross sections and flux computed with transport code with finer energy structure (ECCO 1968-group in this paper).

In order to evaluate the accuracy of self-shielding corrections based on 33-group structure, an additional scheme shown in Figure 2 by blue dashed symbols is used in the present work. Using the multi-group neutron flux ϕ_j and self-shielding corrected cross sections $\tilde{\sigma}_{i,j}$ calculated by transport code in a finer structure (ECCO 1968-group in our studies), we compute 33-group neutron flux by summing neutron flux of which the group j in the finer structure is included in group J of 33-group. The deduced 33-group cross sections are obtained by conserving the same reaction rates.

In the following studies, the infinite dilution multi-group cross sections $\sigma_{i,j}$ and $\sigma_{DPA,i,j}$ are computed by the GROUPT module in NJOY2016.20 with the weighting function iwt8 (i.e. thermal -- 1/E -- fast reactor -- fission & fusion). The self-shielding corrected multi-group cross sections $\tilde{\sigma}_{i,j}$ are calculated by ECCO, of which the methods of self-shielding calculations are presented in Ref. [23].

3. Results and Discussion

3.1 Influence of temperature on recoil energy

Figure 3 shows the average recoil energy of ^{56}Fe for 100 eV, 500 eV, 1 keV, and 5 keV energy neutron elastic scattering with different temperatures. The influence of temperature is more important at lower incident energy. However, due to the threshold energy of atomic displacement, the temperature effect on recoil energy has no influence on DPA computation when the recoil energy is lower than E_d or $2.5E_d$ ($2E_d/0.8$). For neutron elastic scattering shown in Figure 3, different temperatures of ^{56}Fe have the same DPA number (0 DPA) for incident energy lower than 500 eV. For 1 keV neutron, the maximum recoil energy is higher than E_d but lower than $2.5E_d$. Therefore, the DPA number does not change with the temperature. For high incident neutron that the recoil energy of ^{56}Fe can be higher than $2.5E_d$. However, the temperature effect on recoil energy is negligible because of the quite small contribution of the kinetic energy of target ($1.5kT = 0.2$ eV when $T = 1500$ K) before collision, as shown in Figure 3 (d). The average recoil energies with different incident energies and different temperatures are given in Table I. Both Figure 3 and Table I shows that the consideration of the thermal vibration of the target has neglectable influence on DPA computations. By consequence, the DPA cross sections computed by NJOY without considering thermal vibration of the target can be directly used.

Table I. Average recoil energy (in eV) of ^{56}Fe for 100 eV, 500 eV, 1 keV, 5 keV, and 10 keV incident neutron elastic scattering with different temperature

E	100 eV	500 eV	1 keV	5 keV	10 keV
10 K	3.52	17.61	35.22	176.09	352.11
293 K	3.56	17.65	35.25	176.12	352.15
1500 K	3.71	17.80	35.41	176.25	352.37

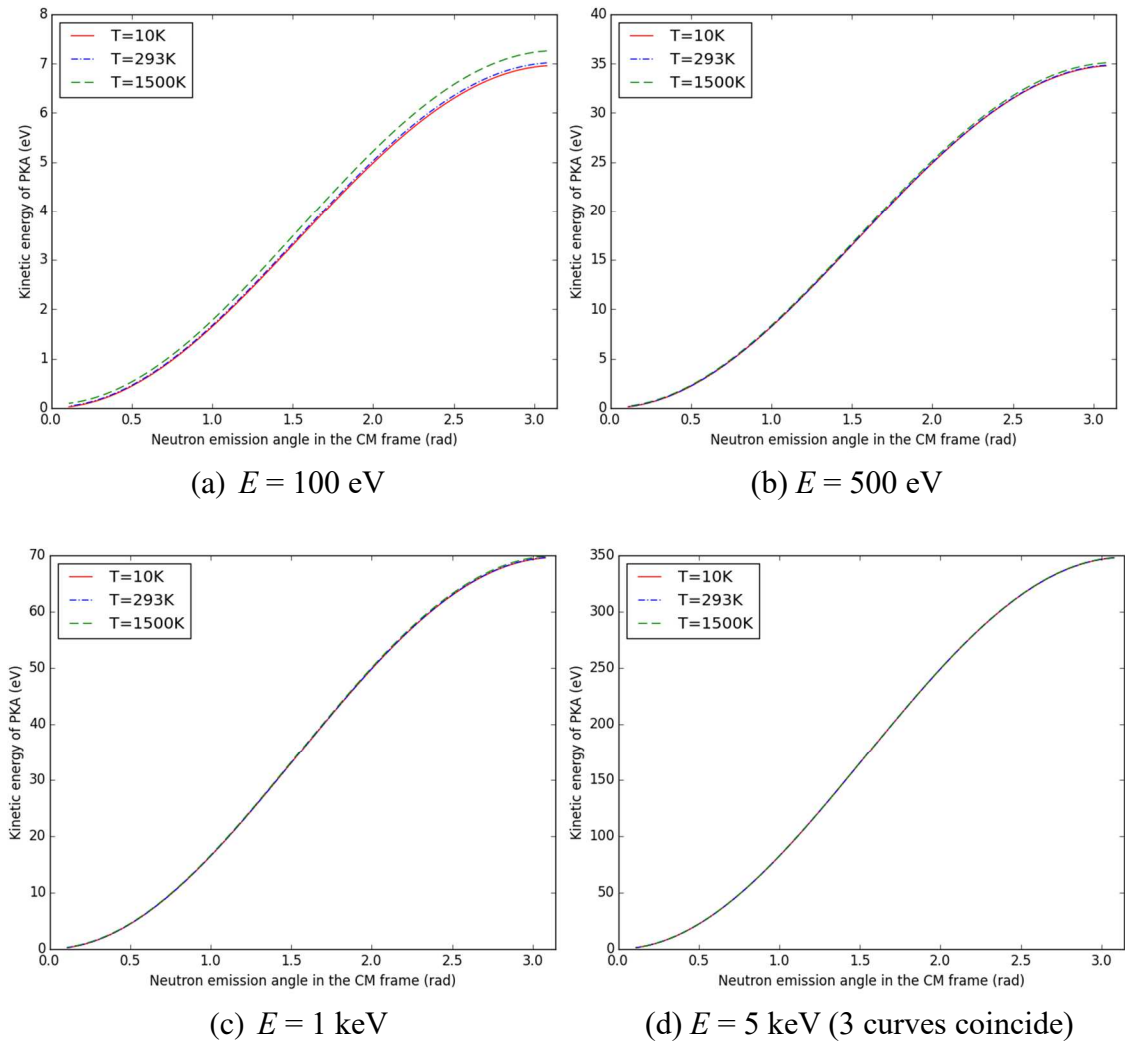


Figure 3. Average PKA energy of ^{56}Fe for 100 eV, 500 eV, 1 keV, and 5 keV incident neutrons with different temperatures of the target

3.2 DPA cross sections and temperature effect

Reaction cross sections depend on the temperature of the material because of the Doppler broadening. Figure 4 shows the total, elastic scattering, inelastic scattering, and capture cross sections (MT1, MT2, MT4, and MT102, respectively) at the reference temperature 293.15 K on the ECCO 1968-group mesh. The ratios of corresponding cross sections at 1500 K to those at 293.15 K (i.e. $\sigma_{i,j}(1500 \text{ K})/\sigma_{i,j}(293.15 \text{ K})$) for ^{56}Fe are shown in Figure 5. The ratios higher than unity because the Doppler broadening enlarges the width (> 1 at two wings of resonances), while the lower than unity ratios are due to the decrease of the peak value (< 1 at centers of resonances). No difference is observed at neutron energy E higher than 1 MeV. The Doppler effect has a strong influence on the resonances of capture cross sections in $1 \text{ keV} < E < 1 \text{ MeV}$, but it influences much less the total cross sections because the elastic scattering is the dominant reaction from 1 keV up to 1 MeV. Only at 1 keV the Doppler effect is important for the total cross section due to the strong resonance of the capture cross

section.

The Doppler effect is more important at lower energy due to larger perturbation of relative velocity. However, Figure 5 shows that the Doppler effect does not change the capture cross section at low energy. Although the dependence of elastic scattering cross section on temperature is evident, the variation of elastic scattering cross section at low energy does not influence the DPA cross sections because the corresponding recoil nuclei or atoms have energies lower than the threshold energy of displacement.

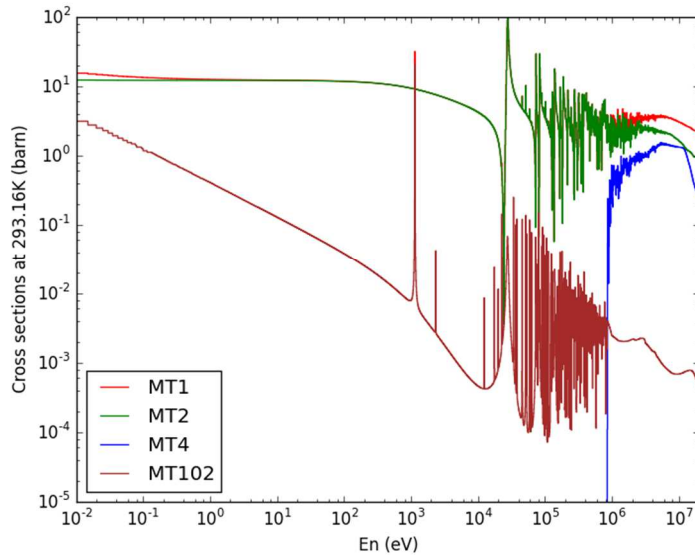


Figure 4. Total, elastic, inelastic, and capture cross sections of ^{56}Fe at 293.15 K.

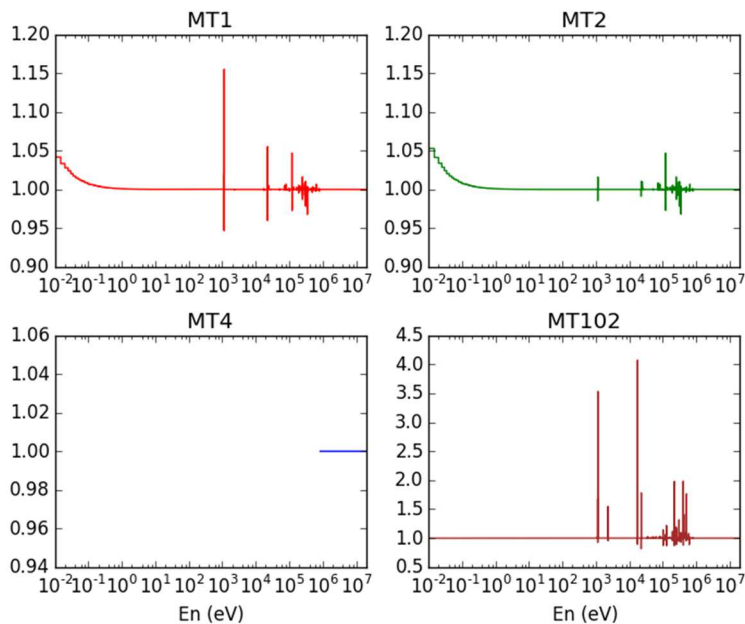


Figure 5. Ratios of cross sections at 1500 K to those at 293.15 K.

Figure 6 illustrates the total, elastic scattering, total inelastic scattering, and disappearance DPA cross sections at 293.15 K. At neutron energy lower than 500 eV, only the disappearance can induce the displacement of atoms because the target nucleus

cannot receive enough energy from scattering reactions. In this region, there is no reaction from MT103 to MT107. Therefore, the capture reaction is the unique reaction that can produce the atomic displacements with ^{57}Fe PKA. From 600 eV to 1 MeV, the elastic scattering has almost 100% contribution to the total DPA. The inelastic scattering should be considered from 1 MeV and it has more important contribution than the elastic scattering for $E > 4$ MeV. The cross section of MT447 increases from 4 MeV because the reaction channels from MT103 to MT107 are open.

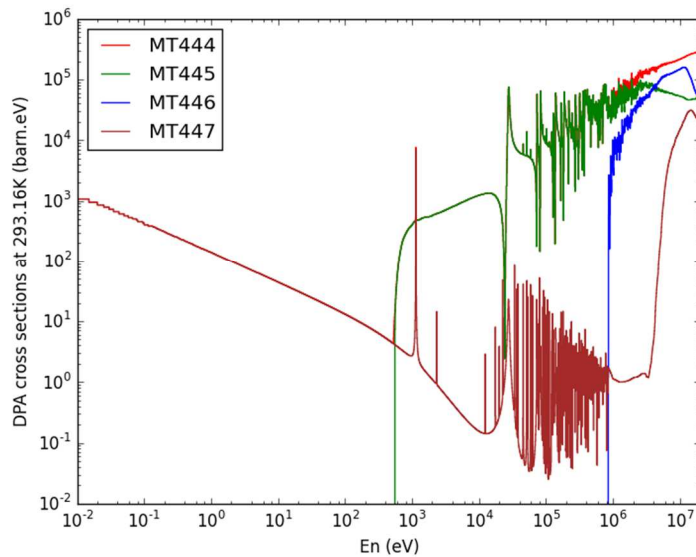


Figure 6. Total, elastic, inelastic, and disappearance DPA cross sections at 293.15 K.

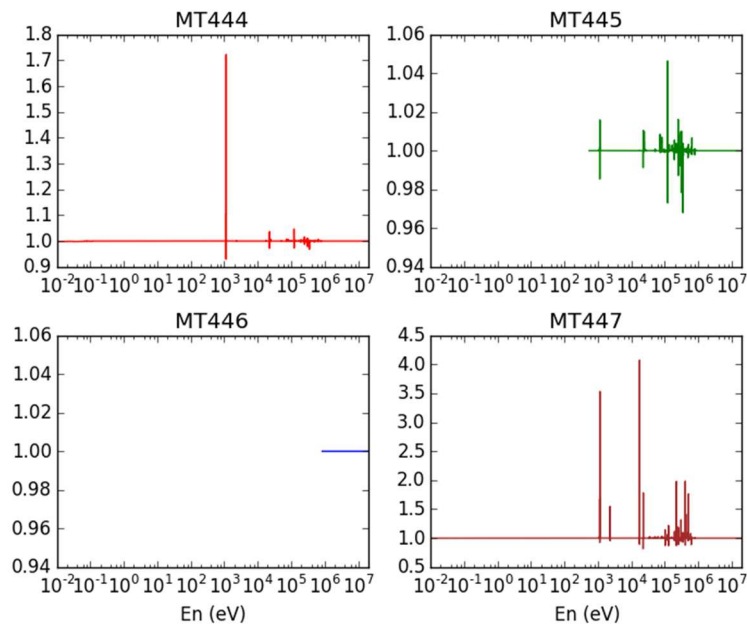


Figure 7. Ratios of DPA cross sections at 1500 K to those at 293.15 K.

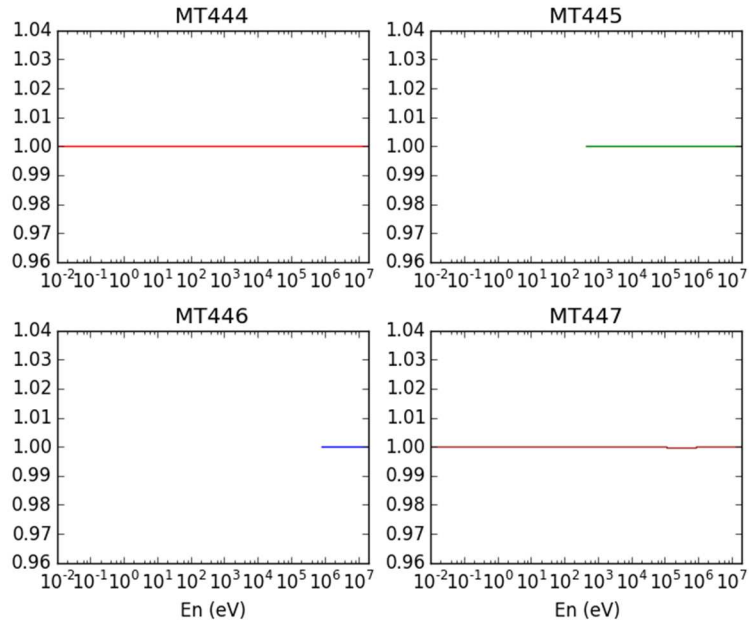


Figure 8. Ratios of DPA cross sections at 1500 K to those at 293.15 K in ECCO 33-group energy structure.

Figure 7 reveals the ratios of DPA cross sections at 1500 K to those at 293.15 K. Same as nuclear cross sections, the Doppler effect has the most important influence on total DPA cross section at 1 keV, at which the capture reaction dominates. Except for this point, the total DPA changes less than 5%, so the DPA should not be sensitive to the temperature. This can be further verified in Figure 8 with ECCO 33-group mesh that only the DPA cross section MT447 changes -0.02% between 0.1 MeV and 1 MeV when the temperature increases from 293 K to 1500 K. In addition, the contribution of MT447 to total DPA is negligible in this region (see Sections 3.3 and 3.4).

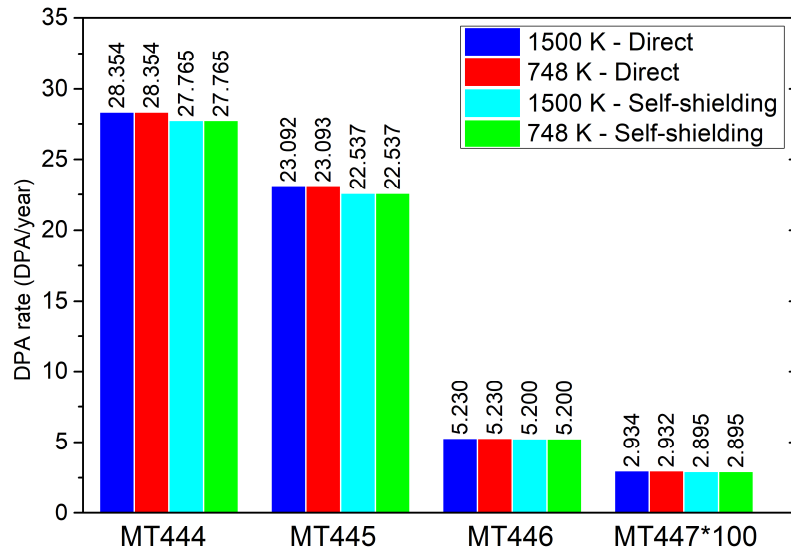


Figure 9. DPA rate (DPA/year) of ^{56}Fe in the ASTRID inner core fuel cladding computed with and without self-shielding treatment and different temperatures. DPA rate induced by reactions other than MT445-447 is 0.002 DPA/year.

Section 3.1 shows that the temperature effect on the recoil energy has neglectable influence on DPA calculations. Only the Doppler effect as illustrated in Figure 7 is considered to show the temperature dependence in ASTRID application. In order to evaluate the influence of Doppler broadening on DPA rate, the example of the ^{56}Fe in the fuel cladding of the ASTRID inner core is taken. The results are given in Figure 9. As expected, the Doppler broadening is negligible for the calculation of DPA. The Doppler broadening has 0.004% contribution to DPA rate in ASTRID inner core when the temperature changes from 748 K to 1500 K. 748 K and 1500 K are the temperatures of fuel cladding and fuel, respectively. Therefore, the temperature effects are not taken into account in the following studies on DPA rates calculations.

3.3 Verification of self-shielding correction

In order to validate the method of self-shielding treatment during DPA calculation with coarse energy grids, the DPA rates computed with ECCO 1968-group and the deduced 33-group calculation (dashed scheme in Figure 2) are compared. The lattice calculations are performed to compute ECCO 1968-group neutron spectrum and self-shielding corrected cross sections. Figure 10 shows the ECCO 1968-group correction coefficients for the total, elastic scattering, total inelastic scattering, and disappearance cross sections. The corresponding reaction cross sections are shown in the same sub-figures to show the resonance self-shielding. The self-shielding corrections on cross sections can be observed in Figure 10 for most resonances.

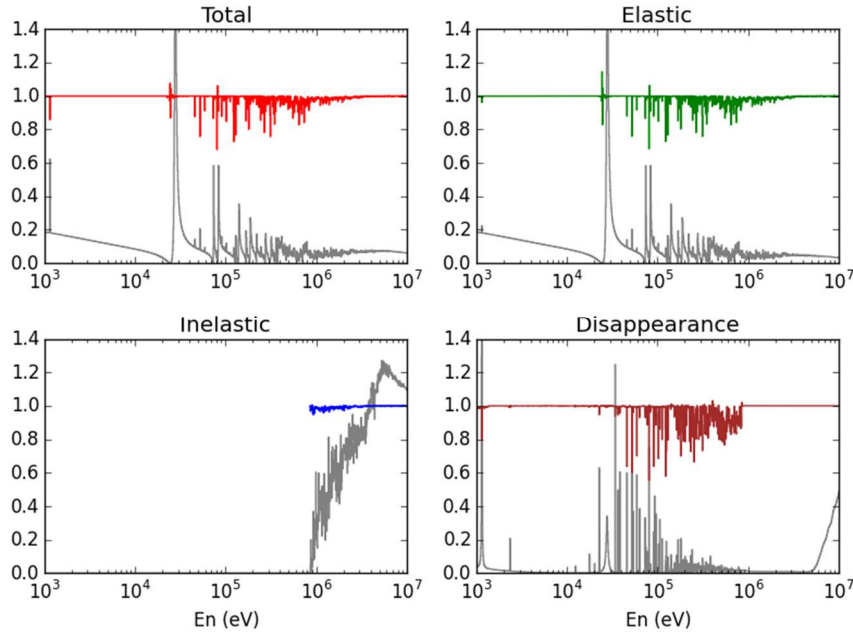


Figure 10. 1968-group correction coefficients for the total, elastic, total inelastic, and disappearance (sum of MT102 to MT120) cross sections versus incident neutron energy. The grey curves are corresponding relative reaction cross sections.

It is noticeable that the small correction coefficients do not mean that the self-shielding is not important at these resonances. In contrast, some of these resonances are so important that the neutron flux is strongly influenced. Because of the strong

influence, the self-shielding corrections are directly accounted in the neutron flux. The valley of the neutron spectrum at 28 keV (shown in Figure 11), which is induced by the strong elastic scattering resonance of ^{56}Fe , is typical for fast reactors. Same phenomena can be found for the two big resonances of elastic scattering at 74 keV and 84 keV.

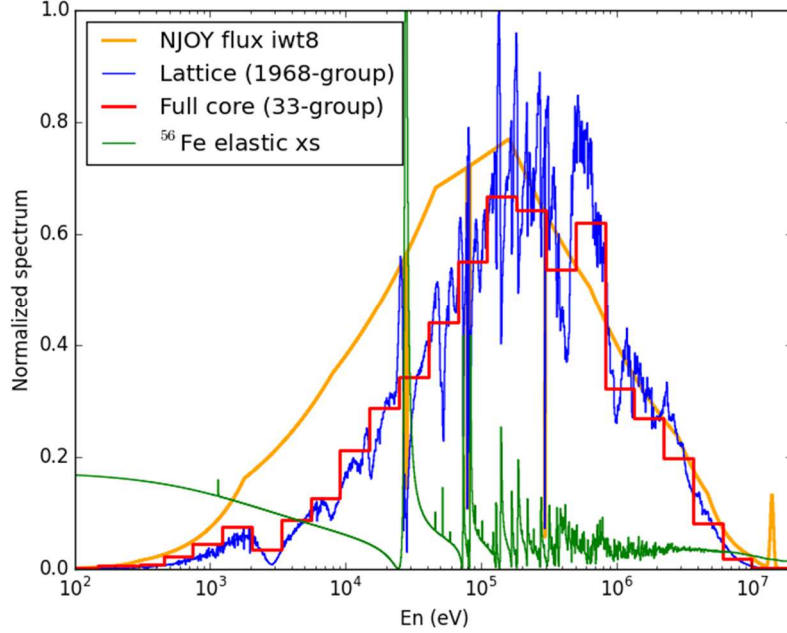


Figure 11. Normalized neutron spectra for NJOY-iwt8, lattice calculation (blue) and full core calculation (red) flux in ASTRID inner core, and the relative elastic scattering cross section of ^{56}Fe .

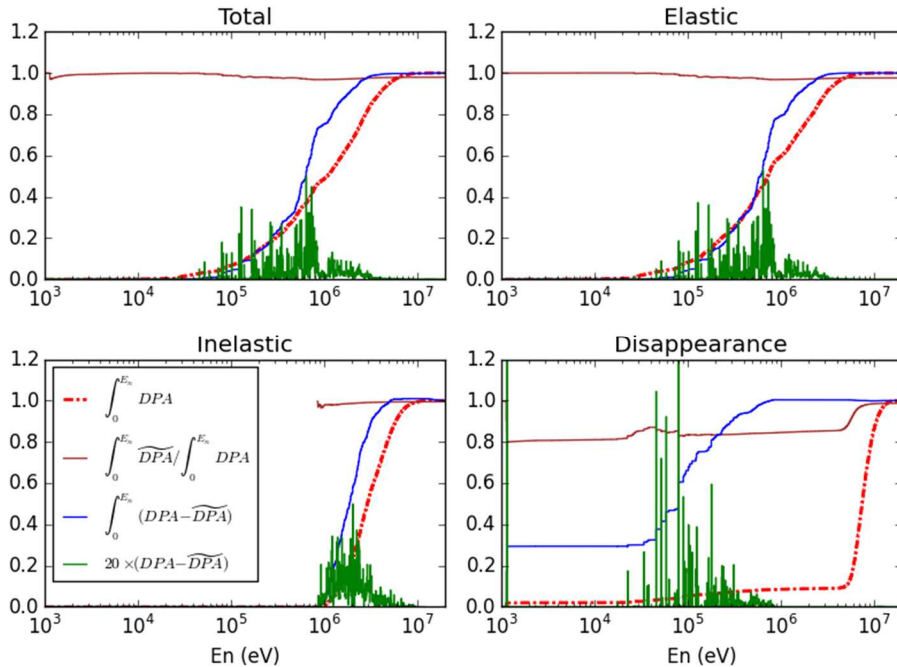


Figure 12. Self-shielding effects with 1968-group energy structure. DPA stands for the relative DPA rate without self-shielding treatment. \overline{DPA} refers to the self-shielding corrected DPA rate. $DPA - \overline{DPA}$ represents the reduction of DPA due to self-shielding, normalized by its integration over whole energy.

The relative accumulated DPA, accumulated self-shielding corrections of DPA, and self-shielding corrections in each group are shown in Figure 12 for 1968-group calculations. Except the correction at 1.15 keV for the (n, γ) reaction, the self-shielding corrections on DPA rates are not found in Figure 12 at incident energies below 50 keV. This is due to the direct corrections on neutron flux, while our calculations with and without self-shielding consideration utilize always the self-shielding corrected neutron spectrum. The self-shielding corrections of cross sections are important for DPA rate at incident energies between 50 keV and 5 MeV.

Figure 13(a) illustrates the DPA rates in the fuel cladding in the ASTRID inner core (lattice calculation) without and with the correction of self-shielding. It is noticeable that the DPA rate induced by reactions other than MT445-447 is only 0.002 DPA/year. Because of the high threshold energies of reactions and the negligible contributions on total DPA, reaction channels excluded in MT445-447 are not treated in self-shielding corrections of PDA rates. The neutron spectrum is the normalized 1968-group spectrum (blue line in Figure 11) multiplied by the total neutron flux of the 33-group spectrum determined in full core calculations (red line in Figure 11). The yellow bars show the negative corrections on DPA rates taking the self-shielding into account. It is noticeable that the DPA computed with total cross sections is less than the sum of three partial values after the self-shielding correction because of the different self-shielding corrections on different cross sections. Therefore, attention should be paid for total DPA rates computed with total DPA cross sections, such as the recent DPA cross sections provided by the Nuclear Energy Agency (NEA) [24].

As pointed out in Figure 13(a), 2.1% relative elastic scattering induced DPA rate is reduced by taking the self-shielding into account. The relative reduction of inelastic scattering is less important due to the null resonant cross section before the threshold energy of reactions. 2.1% total DPA is reduced due to the self-shielding treatment of cross sections with ECCO 1968-group.

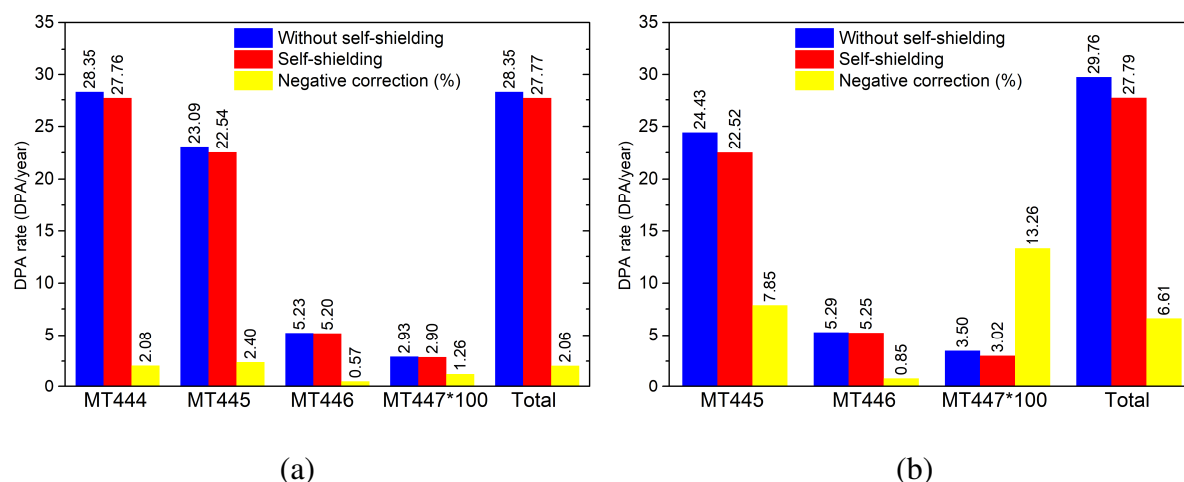


Figure 13. DPA rates (in DPA/year) in the fuel cladding in ASTRID computed with ECCO 1968-group energy structure (a) and the deduced ECCO 33-group calculations (b) illustrated in Figure 2. The absolute neutron spectrum is obtained by multiplying the lattice 1968-group normalized flux and the total flux of full core calculation. The DPA rates of MT447 are multiplied by 100 by the negative corrections are original.

In order to evaluate the accuracy of self-shielding corrected DPA rate based on the ECCO 33-group structure, the calculations illustrated by the dashed scheme in Figure 2 are performed. The result based on 33-group computations are given in Figure 13(b). The self-shielding correction on the disappearance DPA rate is less (more respectively) important than the elastic scattering in 1968-group (33-group respectively). The reason is that the self-shielding corrections on disappearance cross section end at 1 MeV in 1968-group calculations (Figure 12), while the corrections continue to the last group in the deduced 33-group calculations. The correction on inelastic scattering is always less important than those on elastic scattering due to the lack of resonant cross sections in JEFF-3.1.1.

In fact, these correction coefficients used Eq. (17) are not only due to (i) the self-shielding treatment of cross sections but also (ii) the deviations of multi-group cross sections induced by a general weighting function used in NJOY GROUPLR module (orange line in Figure 11). For sufficiently fine mesh such as the ECCO 1968-group, the multi-group cross sections are weighted in a small interval of the resonance, the corrections (ii) of cross sections induced by different weighting function are almost negligible. Due to the fine energy structure, the calculations performed with 1968-group energy structure are considered as standard computations of self-shielding.

Comparing two results shown in Figure 13, it is observed that before the treatment of self-shielding, the DPA rates computed with 33-group are quite different to the reference 1968-group calculations. However, good agreement is shown between the 33-group and the 1968-group calculations after the correction of self-shielding. The correspondence of self-shielding corrected DPA rates between 1968-group calculations and 33-group results shows that the self-shielding proposed in Section 2.3 is valid for ECCO 33-group. In addition, the self-shielding should be taken into account for DPA calculations, especially for coarse energy structures, due to the correction (ii) induced by different weighting functions for computing multi-group cross sections.

3.4 DPA rate in the fuel cladding in ASTRID inner core

Section 3.3 shows that the 33-group structure is suitable to perform the calculation of DPA rates. The full core calculation of ASTRID is performed to compute the ECCO 33-group neutron spectrum and the self-shielding corrected cross sections. The layout of the ASTRID core is shown in Figure 14. The present work aims to compute the DPA rates for the fuel cladding of ASTRID inner core, which is the yellow region pointed out in Figure 14. The corresponding neutron spectrum is shown in Figure 11 by the red line. Figure 15 illustrates the 33-group correction coefficients for the total, elastic scattering, total inelastic scattering, and disappearance cross sections.

The relative accumulated DPA rates, the accumulated self-shielding corrections of DPA rates, and the self-shielding corrections in each group are shown in Figure 16 for the above-mentioned four reactions. Figure 16 shows that the self-shielding between 25 keV and 6 MeV is most important in DPA calculations. Out of this band, the self-shielding corrections of cross sections and DPA calculations are weak due to few resonances and low neutron flux.

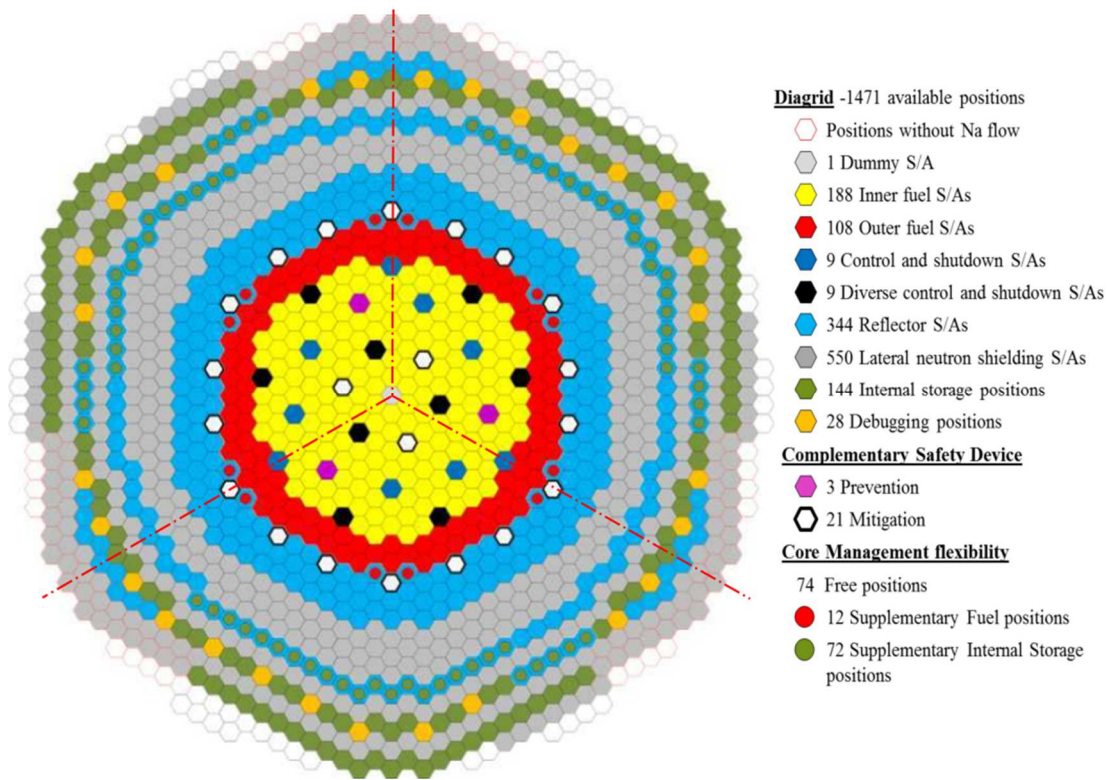


Figure 14. Layout of ASTRID core (3-fold rotational symmetry)

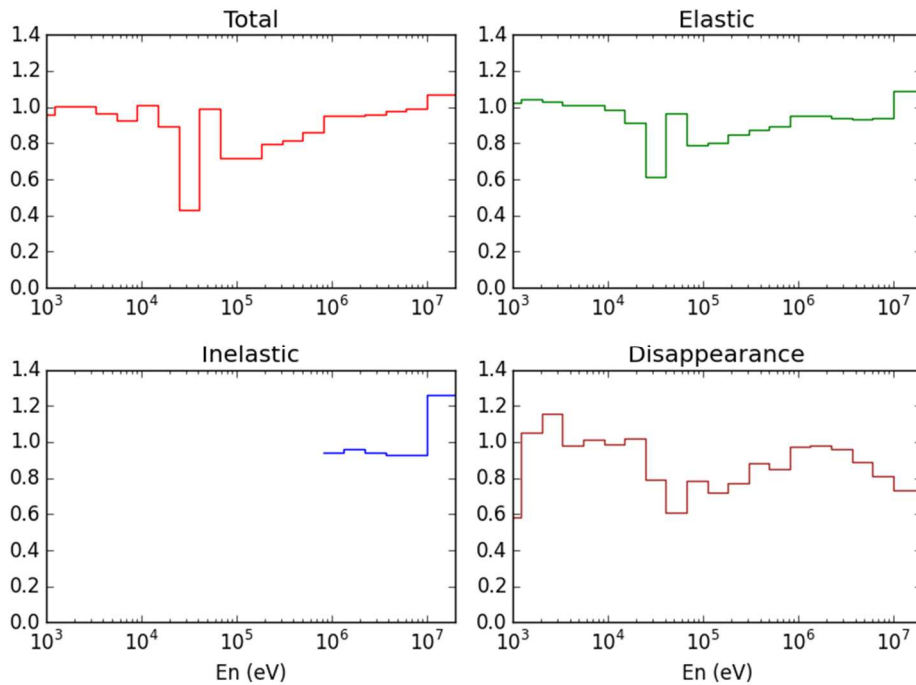


Figure 15. 33-group full core correction coefficients for different cross sections

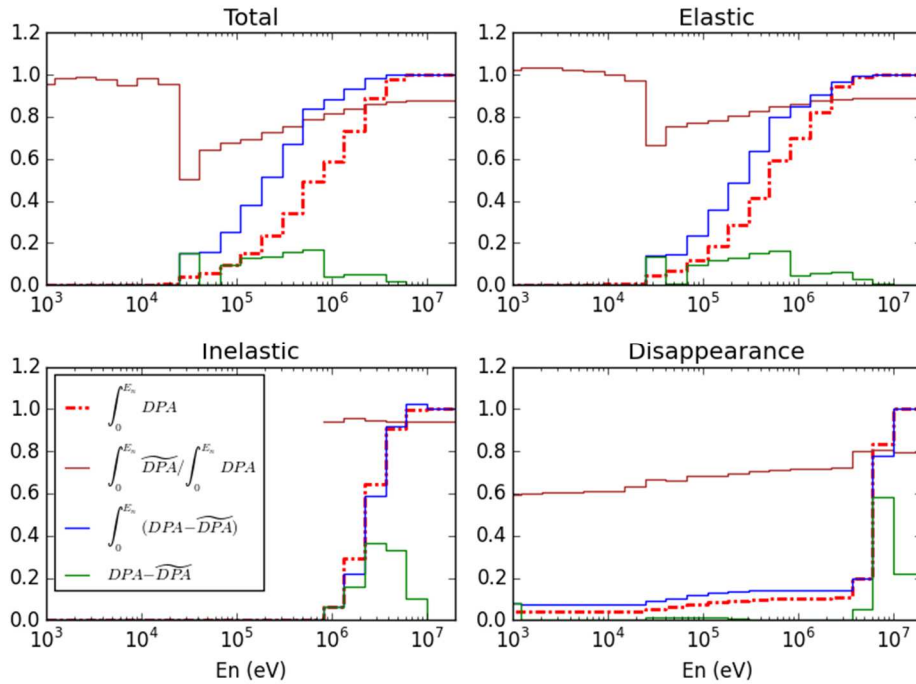


Figure 16. Self-shielding effects with 33-group energy structure. DPA stands for the relative DPA rate without self-shielding treatment of cross sections. \widehat{DPA} refers to the self-shielding corrected DPA rate. $DPA - \widehat{DPA}$ represents the reduction of DPA due to self-shielding, normalized by its integration over whole energy.

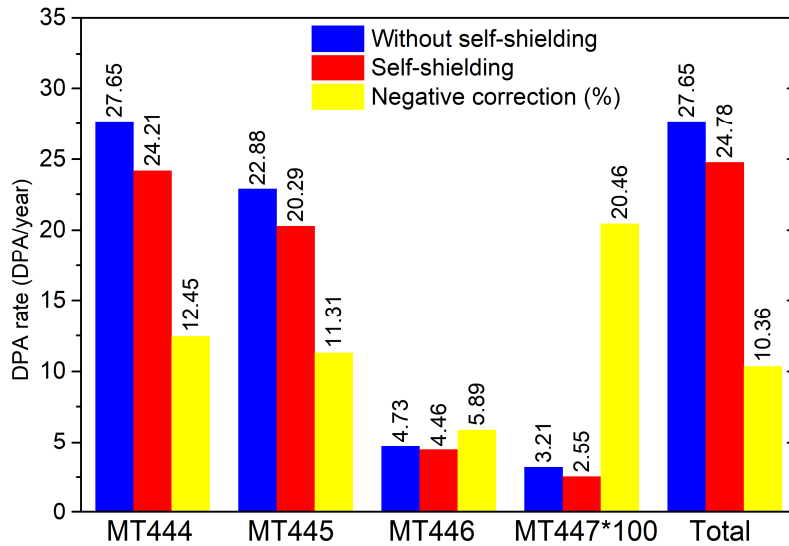


Figure 17. DPA rates (in DPA/year) in the fuel cladding in ASTRID inner core computed with ECCO 33-group full core calculations. DPA rate induced by reactions other than MT445-447 is 0.0098 DPA/year.

The energy band of the self-shielding corrections of cross sections in 1968-group lattice calculations ([50 keV, 5 MeV] shown Figure 12) is included in the correction interval of 33-group full core calculations ([25 keV, 6 MeV] shown Figure 16). For

1968-group, the higher energy of the lower limit of correction is due to the direct correction on neutron flux at low energies at which the resonances are too strong. The lower energy of upper limit of correction is due to fine group mesh while the multi-group cross sections are averaged over a fluctuated flux (see Figure 11) for a coarse mesh such as the ECCO 33-group energy structure.

Figure 17 illustrates the DPA rates in the fuel cladding in the ASTRID inner core without and with the self-shielding corrections of cross sections. The yellow bars point out the negative corrections on DPA calculations taking the corrections of cross sections into account. Same as the results found in Section 3.3, the DPA computed with total cross sections is less than the sum of three partial values after the self-shielding correction because of the different self-shielding corrections on different cross sections. 11% relative elastic scattering induced DPA rate is reduced by taking the self-shielding into account. Because inelastic scattering channels are closed below the minimum threshold energy of 862 keV, the self-shielding corrections in the resonance region below 862 keV have no influence on DPA induced by inelastic scatterings. Therefore, the relative reduction of inelastic scattering is less important than the one of elastic scattering. The self-shielding effect on the disappearance reactions induced DPA is important, but its contribution to total DPA is negligible. 10% total DPA is reduced due to the self-shielding treatment in ECCO 33-group full core calculations. The self-shielding corrected DPA rate is 25 DPA/year, of which 81.9%, 18.0%, and 0.1% are induced by elastic scattering, inelastic scatterings, and disappearance reactions, respectively.

4. Conclusions

DPA is one of the most important parameters that measure the irradiation damage of materials during and after irradiation. DPA is conventionally computed using the DPA cross sections and neutron spectra in reactors. The temperature influences the DPA cross sections through the PKA energy due to the thermal vibration of atoms and the Doppler broadening of reaction cross sections. The influence of the temperature on PKA energy is important at low incident energy. However, low incident energy leads to low PKA energy. Due to the threshold energy of atomic displacement, the temperature has no effect on DPA calculation for low incident energies. For high incident energy, the temperature effect on PKA energy is negligible because the kinetic energy of PKA before collision ($1.5kT$) is too small compared with the incident energy. Consequently, the temperature effect on PKA energy does not change the DPA calculations.

The Doppler effect depends on the resonances of the recoil nucleus. For ^{56}Fe , the Doppler broadening has limited influence on DPA cross sections because of small influence on scattering cross sections above the threshold energies shown in Figure 6. The application in the fuel cladding in the ASTRID inner core shows that the Doppler broadening has less than 0.01% contribution on final DPA computations. Therefore, the temperature dependence of DPA cross sections is negligible for ^{56}Fe .

The self-shielding effects are studied for DPA calculations with both ECCO 1968-group and the deduced 33-group calculations. The reduction of total DPA due to the

correction of cross sections is from both (i) the self-shielding treatment of cross sections and (ii) the deviations of multi-group cross sections induced by a general weighting function in NJOY GROUPT calculations. The self-shielding correction (i) is required only for the deterministic methods, while the correction (ii) exists in both deterministic and stochastic methods. The good agreement between corrected DPA rates computed with the two energy structures validates the accuracy of ECCO 33-group based DPA calculations. Large discrepancies are observed between two structures calculations without self-shielding treatment. This points out that Eq. (17) should be used to compute DPA rates rather than direct calculations with NJOY processed multi-group DPA cross sections, especially for coarse energy structures, whereas the comparisons between 1968-group and the deduced 33-group calculations show that the correction (ii) is much more important than the correction (i) for the 33-group calculations.

Both 33-group full core calculation and 1968-group lattice calculation show that the corrections on total cross sections cannot give the same result as the sum of all the corrected partial DPA rates. 2.3% difference is found between the DPA rate computed with total cross sections and the sum of DPA rates calculated with partial cross sections in 33-group full core calculations. Therefore, attention should be paid for DPA rates calculated with total DPA cross sections, such as the DPA cross sections provided by NEA. The recommended method to compute DPA is the calculation of each reaction using Eq. (17), especially for coarse energy structures. The full core calculations of ^{56}Fe show that the relative reductions off DPA rates due to the corrections on multi-group cross sections are respectively 11.3%, 5.9%, and 20.5% for elastic scattering, inelastic scatterings, and disappearance reactions. These lead to 10.4% correction on total DPA rate. The corrected DPA rate in the fuel cladding of ASTRID reactor is about 25 DPA/year using the NRT-DPA metric. The neutron elastic, inelastic scatterings, and the disappearance reactions induced DPA rates contribute respectively 81.9%, 18.0%, and 0.1% on total DPA rate.

References

- [1] S. J. Zinkle and G. S. Was, "Materials challenges in nuclear energy," *Acta Mater.*, vol. 61, no. 3, pp. 735–758, Feb. 2013.
- [2] M. Chenaud *et al.*, "Status of the ASTRID core at the end of the pre-conceptual design phase 1," *Nucl. Eng. Technol.*, vol. 45, no. 6, pp. 721–730, Nov. 2013.
- [3] F. Gao, D. J. Bacon, P. E. J. Flewitt, and T. A. Lewis, "A molecular dynamics study of temperature effects on defect production by displacement cascades in α -iron," *J. Nucl. Mater.*, vol. 249, no. 1, pp. 77–86, Sep. 1997.
- [4] W. J. Pythian, R. E. Stoller, A. J. E. Foreman, A. F. Calder, and D. J. Bacon, "A comparison of displacement cascades in copper and iron by molecular dynamics and its application to microstructural evolution," *J. Nucl. Mater.*, vol. 223, no. 3, pp. 245–261, Jun. 1995.
- [5] R. E. Stoller, "The role of cascade energy and temperature in primary defect formation in iron," *J. Nucl. Mater.*, vol. 276, no. 1, pp. 22–32, Jan. 2000.
- [6] R. E. Stoller, "Primary Radiation Damage Formation," in *Comprehensive Nuclear*

- Materials*, R. J. M. Konings, Ed. Oxford: Elsevier, 2012, pp. 293–332.
- [7] R. E. MacFarlane and A. C. Kahler, “Methods for Processing ENDF/B-VII with NJOY,” *Nucl. Data Sheets*, vol. 111, no. 12, pp. 2739–2890, Dec. 2010.
- [8] S. Chen and C. Yuan, “Neutronic Analysis on Potential Accident Tolerant Fuel-Cladding Combination U_3Si_2 -FeCrAl,” *Sci. Technol. Nucl. Install.*, vol. 2017, no. 3146985, 2017.
- [9] S. Chen, C. Yuan, and D. Guo, “Radial distributions of power and isotopic concentrations in candidate accident tolerant fuel U_3Si_2 and UO_2/U_3Si_2 fuel pins with FeCrAl cladding,” *Ann. Nucl. Energy*, vol. 124, pp. 460–471, Feb. 2019.
- [10] J. M. Ruggieri *et al.*, “ERANOS 2.1: International Code System for GEN IV Fast Reactor Analysis,” in *Proceedings of ICAPP 06*, Reno, NV USA, 2006, pp. 2432–2439.
- [11] A. Santamarina *et al.*, “The JEFF-3.1.1 Nuclear Data Library,” OECD/NEA, JEFF Report 22, NEA No. 6807, 2009.
- [12] R. E. MacFarlane, D. W. Muir, R. M. Boicourt, A. C. Kahler, and J. L. Conlin, “The NJOY Nuclear Data Processing System, Version 2016,” Los Alamos National Laboratory (LANL), Los Alamos, NM, United States, LA-UR-17-20093, 2016.
- [13] S. Chen, D. Bernard, P. Tamagno, J. Tommasi, S. Bourganel, and G. Noguere, “Irradiation Damage Calculation with Angular Distribution,” *arXiv*, no. 1902.05620, 2019.
- [14] G. H. Kinchin and R. S. Pease, “The Displacement of Atoms in Solids by Radiation,” *Rep Prog Phys*, vol. 18, no. 1, pp. 1–51, 1955.
- [15] J. Lindhard, V. Nielsen, M. Scharff, and P. V. Thomsen, “Integral equations governing radiation effects,” *Mat Fys Medd Dan Vid Selsk*, vol. 33, no. 10, pp. 1–42, 1963.
- [16] M. J. Norgett, M. T. Robinson, and I. M. Torrens, “A proposed method of calculating displacement dose rates,” *Nucl. Eng. Des.*, vol. 33, no. 1, pp. 50–54, 1975.
- [17] M. T. Robinson and I. M. Torrens, “Computer simulation of atomic-displacement cascades in solids in the binary-collision approximation,” *Phys. Rev. B*, vol. 9, no. 12, pp. 5008–5024, Jun. 1974.
- [18] M. T. Robinson, “Energy Dependence of Neutron Radiation Damage in Solids,” *Nucl. Fusion React.*, pp. 364–378, 1970.
- [19] ASTM E693-94, *Standard Practice for Characterizing Neutron Exposures in Iron and Low Alloy Steels in Terms of Displacements Per Atom (DPA), E706(ID)*. West Conshohocken, PA: ASTM International, 2001.
- [20] R. S. Averback, R. Benedek, and K. L. Merkle, “Ion-irradiation studies of the damage function of copper and silver,” *Phys. Rev. B*, vol. 18, no. 8, p. 4156, 1978.
- [21] K. Nordlund *et al.*, “Improving atomic displacement and replacement calculations with physically realistic damage models,” *Nat. Commun.*, vol. 9, no. 1, 2018.
- [22] S. Chen, D. Bernard, P. Tamagno, and C. De Saint Jean, “Calculation and Verification of Irradiation Damage Cross Section with Energy-Angular Distribution,” *arXiv*, no. 1902.04889, 2019.

- [23] G. Rimpault, P. Ribon, M. Grimstone, C. Dean, B. Thom, and C. Cavarec, "Validation of new sub-group algorithms for resonance self-shielding in heterogeneous structures," Nuclear Energy Agency of the OECD (NEA), Saclay, France, Seminar on NJOY and THEMIS, INIS-XN--305, 1989.
- [24] NEA, "JEFF-3.3/DPA: Atomic displacement (radiation damage) cross sections," <https://www.oecd-nea.org/dbdata/jeff/jeff33/index.html>, Nov. 2017.